ELSEVIER

Composite Structures 50 (2000) 1–15

COMPOSITE STRUCTURES

www.elsevier.com/locate/compstruct

First-order zig-zag sublaminate plate theory and finite element model for laminated composite and sandwich panels

Y.B. Cho, R.C. Averill *

Department of Materials Science and Mechanics, Michigan State University, East Lansing, MI 48824 1226, USA

Abstract

A refined laminated plate theory and three-dimensional finite element based on first-order zig-zag sublaminate approximations has been developed. The in-plane displacement fields in each sublaminate are assumed to be piecewise linear functions and vary in a zig-zag fashion through-the-thickness of the sublaminate. The zig-zag functions are evaluated by enforcing the continuity of transverse shear stresses at layer interfaces. This in-plane displacement field assumption accounts for discrete layer effects without increasing the number of degrees of freedom as the number of layers is increased. The transverse displacement field is assumed to vary linearly through-the-thickness. The transverse normal strain predictions are improved by assuming a constant variation of transverse normal stress in each sublaminate. In the computational model, each finite element represents one sublaminate. The finite element is developed with the topology of an eight-noded brick, allowing the thickness of the plate to be discretized into several elements, or sublaminates, where each sublaminate can contain more than one physical layer. Each node has five engineering degrees of freedom, three translations and two rotations. Thus, this element can be conveniently implemented into general purpose finite element codes. The element stiffness coefficients are integrated exactly, yet the element exhibits no shear locking due to the use of an interdependent interpolation scheme and consistent shear strain fields. Numerical performance of the current element is investigated for a composite armored vehicle panel and a sandwich panel. These tests demonstrate that the element is very accurate and robust. © 2000 Published by Elsevier Science Ltd.

Keywords: First-order zig-zag sublaminate plate theory; Finite element model

1. Introduction

Fiber reinforced laminated composites are often used in structural members due to better stiffness-to-weight and strength-to-weight ratios than those of conventional monolithic materials. Common characteristics of laminated composites are that the material properties are orthotropic in the laminate plane, the ratio of transverse shear modulus to in-plane modulus is low and layers are laminated through-the-thickness. Therefore, unlike homogeneous isotropic materials, the behavior of laminated composites is unique and complicated at both the global and the local levels. The early laminated composites were applied to thin structures and were designed to withstand mainly in-plane tension loads. But recently they are also employed for primary load-carrying structural members in automobile front aprons, bridge frames, submarine hulls and aircraft because of advances in their manufacturing techniques. Such recent applications of composite materials involve the use of thick-section laminates and/or sandwich construction that contains a thick core between face sheets. Such structures are typically designed to withstand complex mechanical loading states and harsh environmental conditions.

Many plate theories have been developed on the basis of various kinematic assumptions to predict the response of laminates more accurately. Comprehensive reviews of the literature on the development of modern plate theories have recently been carried out by several authors [1–6]. Plate theories are usually classified by the form of their assumed displacement fields. Such models can roughly be divided into three categories: equivalent single layer theories, layerwise theories, and zig-zag in-plane displacement theories. In the equivalent single layer approach, the material properties of all the layers are 'smeared', and the laminate is modeled as an equivalent single anisotropic layer. The most popular of these theories is the first-order shear deformation theory (FSDT) [7], which assumes that a line originally straight and normal to the reference surface remains straight

* Corresponding author.

0263-8223/00/$ - see front matter © 2000 Published by Elsevier Science Ltd.
PII: S0263-8223(99)00063-X

during deformation but not necessarily perpendicular to the reference surface. This theory yields good predictions of overall laminate behavior (e.g., deflections, natural frequencies, and buckling loads) and in-plane stresses provided the plate is thin and the material properties of adjacent layers do not differ significantly. However, FSDT does not account for warpage of the cross section, which may be significant in laminated composites. In order to reduce the inaccuracies of the FSDT, higher-order shear deformation theories (HSDT) were proposed (e.g., [8–10]). In these models, it is assumed that the displacements are of higher-order polynomial form and are C^1 continuous through-the-thickness. These assumptions permit nonlinear variations of displacements, strains and stresses through-the-thickness, and thus warpage of the cross section. However, even though they often can predict well the gross behavior of thin and some moderately thick laminates, all equivalent single layer theories have a common shortcoming. They are unable to account for the sometimes severe discontinuities in transverse shear strains that occur at interfaces between two adjacent layers with drastically different stiffness properties. In these cases, the local deformations and stresses, and sometimes even the overall laminate response, are not well predicted.

In an effort to overcome the shortcomings of the equivalent single layer approach, discrete-layer (or layerwise) theories have been proposed (e.g., [11–14]). These theories are based on a unique displacement field for each layer and enforce interlaminar continuity of displacements and sometimes of transverse stresses, as well. These theories predict excellent global and local distributions of in-plane and out-of-plane displacements and stresses. The major shortcoming in these theories is their large computational expense, for as the number of layers increases, the number of degrees of freedom increases proportionally.

A new class of laminate theory, called here the first-order zig-zag theory (FZZT), was developed by DiSciuva in the mid 1980s [15,16]. In this theory, in-plane displacements in a laminate are assumed to be piecewise (layerwise) linear and continuous through-the-thickness, yet the total number of degrees of freedom is only five (not dependent on the number of layers). This is accomplished by analytically satisfying the transverse shear stress continuity conditions at each interface in the laminate. This theory was shown to be very accurate for many cases, especially symmetric laminates. On the basis of the concept introduced in [15,16], DiSciuva as well as other researchers made significant improvements to the FZZT [17–23]. The primary improvement was achieved by superimposing a piecewise linear variation of in-plane displacements on a continuous cubic function of the transverse coordinate [17,18,21–23], creating a displacement field that can better account for the warping that occurs during bending of unsymmetric laminates. These latter theories, denoted here as higher-order zig-zag theories (HZZT), also satisfy the homogeneous shear traction boundary conditions at the top and bottom surfaces of the laminate in order to maintain the number of degrees of freedom at five. This class of theories appears to have an ideal combination of accuracy and efficiency, making them well-suited for use in computational simulations. However, these theories have the unfortunate shortcoming that the transverse deflection degree of freedom w_0 is required to be C^1 continuous, so that Hermitian-type interpolation of w_0 must be used within the finite element models [15,17]. Thus, additional rotational degrees of freedom (gradients of w_0) are present in the finite element models, making it inconvenient, if not impossible, to implement the finite element models based on these theories into commercial finite element software packages that allow only six degrees of freedom – three translations and three rotations.

Averill proposed a generalized form of the first-order zig-zag theory [20] and a generalized form of the higher-order zig-zag theory [21] for beams to alleviate the requirement of C^1 continuity on the transverse deflection. A new variable was introduced along with an associated constraint condition which was enforced by employing an interdependent (anisoparametric) element interpolation scheme and the penalty method. On the basis of the theories, C^0 two-noded elements were developed. These elements were shown to be simple, robust and accurate for application to thick and thin laminated beams. However, these models still contained one additional rotational degree of freedom, and it was found that for very thick and complex laminates, more refinement through-the-thickness was needed.

Yip and Averill developed a model for laminated beams [22] and plates [23] that combined the benefits of the discrete-layerwise and higher-order zig-zag theories. This model allows the laminate to be subdivided into a number of sublaminates, with each sublaminate containing several, even many, physical layers. Within each sublaminate, very accurate higher-order zig-zag kinematics are assumed in which degrees of freedom describe displacements, rotations, and transverse shear stresses (tractions or interlaminar stresses) at the top and bottom surfaces of the sublaminate. Each finite element represents one sublaminate, and, if cast in the form of a four-noded quadrilateral (for beams) or an eight-noded brick (for plates), refinement of a model by through-thickness discretization can be achieved without the use of any special constraints. When only one sublaminate is used through the entire thickness of the laminate, nodal degrees of freedom are three translations and two rotations. However, when multiple elements (sublaminates) are needed to model a laminate, additional shear stress degrees of freedom are present,

making the element unsuitable for implementation into many of the current commercial finite element codes.

In this paper, a refined plate theory based on sublaminate linear zig-zag kinematics and a new 3-D finite element based on that theory are developed. The new C^0 element contains eight nodes of which each has only five engineering degrees of freedom – three translations and two rotations. The element is shown to be accurate, simple to use, and compatible with the requirements of commercial finite element codes.

2. Formulation of the theory

In this plate theory, a laminate will be modeled as M sublaminates, and each sublaminate is assumed to consist of N_m perfectly bonded layers which have independent thickness and independent stiffness properties. The total number of layers, N, in the laminate is given by

$$N = \sum_{m=1}^{M} N_m. \tag{1}$$

The global Z-axis is taken perpendicular to the in-plane X, Y coordinate axes and has its origin at the bottom of the laminate, while z is a local sublaminate coordinate in the direction of Z with its origin at the bottom of the sublaminate (see Fig. 1). In the following derivation all expressions are related to the mth sublaminate in order to facilitate the development of a computationally convenient finite element model. All indices indicating the sublaminate number are omitted for brevity.

The constitutive relations for a three-dimensional stress state in the kth layer of the mth sublaminate can be written as

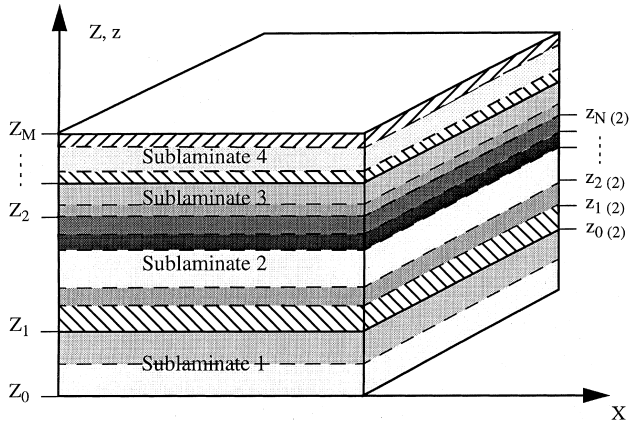

Fig. 1. Schematic representation of sublaminate and layer divisions in the laminated plate theory.

$$\begin{Bmatrix} \sigma_{xx}^{(k)} \\ \sigma_{yy}^{(k)} \\ \sigma_{zz}^{(k)} \\ \sigma_{yz}^{(k)} \\ \sigma_{zx}^{(k)} \\ \sigma_{xy}^{(k)} \end{Bmatrix} = \begin{bmatrix} C_{11}^{(k)} & C_{12}^{(k)} & C_{13}^{(k)} & 0 & 0 & C_{16}^{(k)} \\ C_{12}^{(k)} & C_{22}^{(k)} & C_{23}^{(k)} & 0 & 0 & C_{26}^{(k)} \\ C_{13}^{(k)} & C_{23}^{(k)} & C_{33}^{(k)} & 0 & 0 & C_{36}^{(k)} \\ 0 & 0 & 0 & C_{44}^{(k)} & C_{45}^{(k)} & 0 \\ 0 & 0 & 0 & C_{45}^{(k)} & C_{55}^{(k)} & 0 \\ C_{16}^{(k)} & C_{26}^{(k)} & C_{36}^{(k)} & 0 & 0 & C_{66}^{(k)} \end{bmatrix} \begin{Bmatrix} \varepsilon_{xx}^{(k)} \\ \varepsilon_{yy}^{(k)} \\ \varepsilon_{zz}^{(k)} \\ \gamma_{yz}^{(k)} \\ \gamma_{zx}^{(k)} \\ \gamma_{xy}^{(k)} \end{Bmatrix}. \tag{2}$$

For most practical laminated composites, the 13 coefficients of the material stiffness matrix are obtained from nine independent material constants and a transformation law.

The sublaminate displacement fields are initially assumed in the following form:

$$\begin{aligned} u_x^{(k)}(x,y,z,t) &= u_b + z\psi_x + \sum_{i=1}^{k-1}(z-z_i)\xi_i, \\ u_y^{(k)}(x,y,z,t) &= v_b + z\psi_y + \sum_{i=1}^{k-1}(z-z_i)\eta_i, \\ u_z^{(k)}(x,y,z,t) &= w_b\left(1-\frac{z}{h}\right) + w_t\left(\frac{z}{h}\right), \end{aligned} \tag{3}$$

where h is the thickness of the sublaminate, u_b and v_b are the axial displacements in x and y directions, respectively, at $z=0$, ψ_x and ψ_y the rotations of the normal at $z=0$, and w_b and w_t are the transverse deflections of the bottom and top surfaces, respectively, of the mth sublaminate. Thus, it is assumed that $u_x^{(k)}$ and $u_y^{(k)}$ vary in a piecewise linear fashion through-the-thickness of a sublaminate and $u_z^{(k)}$ varies linearly through-the-thickness. The parameters ξ_i and η_i in Eq. (3) are eliminated by enforcing the continuity of shear stress at each interface [15,16]. The shear stress continuity condition at the kth interface can be expressed as

$$\sigma_{yz}^{(k)} = \sigma_{yz}^{(k+1)}, \qquad \sigma_{zx}^{(k)} = \sigma_{zx}^{(k+1)}. \tag{4}$$

Assuming that infinitesimal strain theory holds, the form of the assumed displacement fields in Eq. (3) is such that the in-plane displacements $u_x^{(k)}$ and $u_y^{(k)}$ contribute only constant (i.e., no variation in z) terms to the transverse shear stresses, $\sigma_{yz}^{(k)}$ and $\sigma_{xz}^{(k)}$. For consistency, then, the transverse displacement $u_z^{(k)}$ should also contribute only constant terms to these stress components. In order to achieve this consistency, terms in the transverse shear strain expressions that involve the transverse displacement variables are evaluated at the mid-plane of the sublaminate, thereby taking a thickness-averaged

value of these terms. This approach is equivalent to ignoring the effect of transverse normal strain on the transverse shear strains, a very good assumption for most laminates. Thus, the transverse shear strains in the kth layer are

$$\gamma_{zx}^{(k)} = \psi_x + \sum_{i=1}^{k-1}\xi_i + \frac{1}{2}\left(\frac{\partial w_b}{\partial x} + \frac{\partial w_t}{\partial x}\right),$$
$$\gamma_{yz}^{(k)} = \psi_y + \sum_{i=1}^{k-1}\eta_i + \frac{1}{2}\left(\frac{\partial w_b}{\partial y} + \frac{\partial w_t}{\partial y}\right). \tag{5}$$

Using Eqs. (2), (4), (5), ξ_i and η_i are then found to be

$$\xi_i = c_i\left\{\psi_y + \frac{1}{2}\left(\frac{\partial w_b}{\partial y} + \frac{\partial w_t}{\partial y}\right)\right\} + d_i\left\{\psi_x + \frac{1}{2}\left(\frac{\partial w_b}{\partial x} + \frac{\partial w_t}{\partial x}\right)\right\},$$
$$\eta_i = a_i\left\{\psi_y + \frac{1}{2}\left(\frac{\partial w_b}{\partial y} + \frac{\partial w_t}{\partial y}\right)\right\} + b_i\left\{\psi_x + \frac{1}{2}\left(\frac{\partial w_b}{\partial x} + \frac{\partial w_t}{\partial x}\right)\right\}, \tag{6}$$

where

$$a_i = \hat{a}_i\left(1 + \sum_{j=1}^{i-1}a_j\right) + \hat{b}_i\sum_{j=1}^{i-1}c_j, \quad b_i = \hat{b}_i\left(1 + \sum_{j=1}^{i-1}d_j\right) + \hat{a}_i\sum_{j=1}^{i-1}b_j,$$
$$c_i = \hat{c}_i\left(1 + \sum_{j=1}^{i-1}a_j\right) + \hat{d}_i\sum_{j=1}^{i-1}c_j, \quad d_i = \hat{d}_i\left(1 + \sum_{j=1}^{i-1}d_j\right) + \hat{c}_i\sum_{j=1}^{i-1}b_j, \tag{7}$$

$$\hat{a}_k = \frac{1}{\Delta_{k+1}}\left(C_{55}^{(k+1)}C_{44}^{(k)} - C_{45}^{(k+1)}C_{45}^{(k)}\right) - 1,$$
$$\hat{b}_k = \frac{1}{\Delta_{k+1}}\left(C_{55}^{(k+1)}C_{45}^{(k)} - C_{45}^{(k+1)}C_{55}^{(k)}\right),$$
$$\hat{c}_k = \frac{1}{\Delta_{k+1}}\left(C_{44}^{(k+1)}C_{45}^{(k)} - C_{45}^{(k+1)}C_{44}^{(k)}\right),$$
$$\hat{d}_k = \frac{1}{\Delta_{k+1}}\left(C_{44}^{(k+1)}C_{55}^{(k)} - C_{45}^{(k+1)}C_{45}^{(k)}\right) - 1,$$
$$\Delta_{k+1} = C_{44}^{(k+1)}C_{55}^{(k+1)} - \left(C_{45}^{(k+1)}\right)^2. \tag{8}$$

From Eqs. (6)–(8) it can be seen that ξ_i and η_i depend on the ratios of shear properties between adjacent layers and the shear deformation in each sublaminate. If either of these quantities is small, then discrete-layer effects will also be small.

The rotational variables ψ_x and ψ_y in the displacement fields are now eliminated by introducing the variables u_t and v_t, the in-plane translations at the top surface of the sublaminate [22,23], in order to expedite the development of versatile finite element models. Thus, rather than describing the in-plane displacement field by a translation and rotation at one point, it can more conveniently be described here by the translation at two points.

The displacement fields must be further manipulated in order to develop a C^0 finite element. Because the derivatives of transverse deflections, $\partial w_b/\partial x$, $\partial w_t/\partial x$, $\partial w_b/\partial y$ and $\partial w_t/\partial y$ appear in the displacement field, their second derivatives will be present in the strain energy functional. C^1 continuity of w_b and w_t is thus required. It is desirable to alleviate such a requirement by introducing new rotational degrees of freedom as follows

$$\frac{\partial w_b}{\partial x} = -\theta_{yb}, \quad \frac{\partial w_t}{\partial x} = -\theta_{yt},$$
$$\frac{\partial w_b}{\partial y} = \theta_{xb}, \quad \frac{\partial w_t}{\partial y} = \theta_{xt}. \tag{9}$$

These relationships will be constrained in the strain energy via the penalty method. Therefore, the displacement fields can be written as follows:

$$u_x^{(k)} = \bar{u}_{\alpha\beta}\Phi_{\alpha\beta}^{(k)}, \quad u_y^{(k)} = \bar{u}_{\alpha\beta}\Psi_{\alpha\beta}^{(k)},$$
$$u_z^{(k)} = w_\beta\Omega_\beta, \qquad \alpha = 1,\ldots,4;\ \beta = 1,2, \tag{10}$$

where the index β is used to denote the top and bottom of the sublaminate with 1: bottom and 2: top, and, $\Phi_{\alpha\beta}^{(k)}$, $\Psi_{\alpha\beta}^{(k)}$ and Ω_β are shape functions in the thickness direction. Unless noted otherwise, summation on repeated indices is implied. The variables $\bar{u}_{\alpha\beta}$ are

$$\bar{u}_{1\beta} = u_\beta, \quad \bar{u}_{2\beta} = v_\beta, \quad \bar{u}_{3\beta} = \theta_{x\beta}, \quad \bar{u}_{4\beta} = \theta_{y\beta}. \tag{11}$$

Thus, the strains are obtained from Eq. (10) as

$$\varepsilon_{xx}^{(k)} = \bar{u}_{\alpha\beta,x}\Phi_{\alpha\beta}^{(k)}, \quad \varepsilon_{yy}^{(k)} = \bar{u}_{\alpha\beta,y}\Psi_{\alpha\beta}^{(k)}, \quad \varepsilon_{zz}^{(k)} = w_\beta\Omega_{\beta,z},$$
$$\gamma_{yz}^{(k)} = \bar{u}_{\alpha\beta}\Psi_{\alpha\beta,z}^{(k)} + w_{\beta,y}\Omega_\beta|_{z=h/2},$$
$$\gamma_{xz}^{(k)} = \bar{u}_{\alpha\beta}\Phi_{\alpha\beta,z}^{(k)} + w_{\beta,x}\Omega_\beta|_{z=h/2},$$
$$\gamma_{xy}^{(k)} = \bar{u}_{\alpha\beta,y}\Phi_{\alpha\beta}^{(k)} + \bar{u}_{\alpha\beta,x}\Psi_{\alpha\beta}^{(k)},$$
$$\alpha = 1,\ldots,4;\ \beta = 1,2, \tag{12}$$

where tensor notations are employed and a comma in the subscript implies partial differentiation. In Eq. (12), the contributions of the transverse deflection to the transverse shear strains $\gamma_{yz}^{(k)}$, and $\gamma_{xz}^{(k)}$ are evaluated at the middle of the sublaminate to ensure constant shear stresses through-the-thickness of a sublaminate (as discussed previously).

The transverse normal strain is constant in a sublaminate. This assumption may give rise to substantial errors in composites that have a soft core or layer. Consider a composite composed of three layers, one of which is very compliant. When the composite is under loading as shown in Fig. 2(a), the uniform transverse normal strain distribution through-the-thickness is predicted from Eq. (12) as in Fig. 2(b). However, the actual distribution is not uniform. Thus, it is desirable to improve the distribution of the transverse normal strain through-the-thickness. The improvement can be achieved by instead assuming a constant transverse normal stress, $\overline{\sigma_{zz}}$, through-the-thickness of a sublaminate. $\overline{\sigma_{zz}}$ can be determined using Reissner's mixed

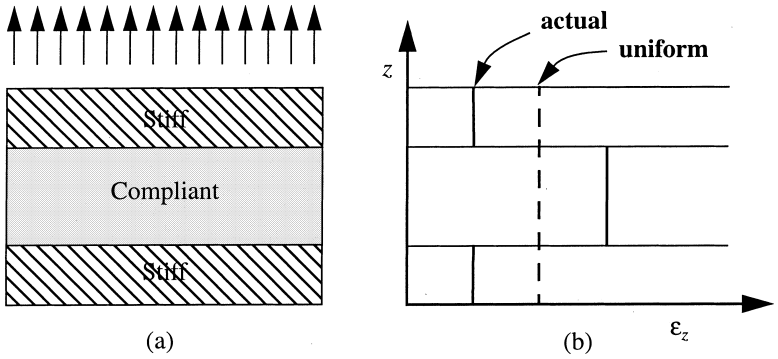

Fig. 2. (a) A composite under transverse tension load and (b) the corresponding transverse strain distribution through the thickness.

variational principle [24]. From Eq. (2), the transverse normal strain is obtained as

$$\bar{\varepsilon}_{zz}^{(k)} = -\frac{C_{13}^{(k)}}{C_{33}^{(k)}}\varepsilon_{xx}^{(k)} - \frac{C_{23}^{(k)}}{C_{33}^{(k)}}\varepsilon_{yy}^{(k)} - \frac{C_{36}^{(k)}}{C_{33}^{(k)}}\gamma_{xy}^{(k)} + \frac{1}{C_{33}^{(k)}}\overline{\sigma_{zz}}. \tag{13}$$

$\overline{\sigma_{zz}}$ is then determined analytically from the following relation:

$$0 = \sum_{k=1}^{N}\int_{z_{k-1}}^{z_k}\left(\bar{\varepsilon}_{zz}^{(k)} - \frac{w_t - w_b}{h}\right)\mathrm{d}z. \tag{14}$$

The constant transverse normal stress $\overline{\sigma_{zz}}$ is found to be

$$\begin{aligned}\overline{\sigma_{zz}} = {} & \frac{\partial u_b}{\partial x}(P_1 + S_6) + \frac{\partial u_t}{\partial x}(P_2 - S_6) + \frac{\partial v_b}{\partial x}(P_3 + S_7) \\ & + \frac{\partial v_t}{\partial x}(-P_3 + S_8) + \frac{\partial \theta_{yb}}{\partial x}(P_4 + S_9) \\ & + \frac{\partial \theta_{yt}}{\partial x}(P_4 + S_9) + \frac{\partial \theta_{xb}}{\partial x}(P_5 + S_{10}) \\ & + \frac{\partial \theta_{xt}}{\partial x}(P_5 + S_{10}) + \frac{\partial u_b}{\partial y}(Q_1 + S_1) \\ & + \frac{\partial u_t}{\partial y}(-Q_1 + S_2) + \frac{\partial v_b}{\partial y}(Q_2 + S_3) \\ & + \frac{\partial v_t}{\partial y}(Q_3 - S_3) + \frac{\partial \theta_{yb}}{\partial y}(Q_4 + S_4) \\ & + \frac{\partial \theta_{yt}}{\partial y}(Q_4 + S_4) + \frac{\partial \theta_{xb}}{\partial y}(Q_5 + S_5) \\ & + \frac{\partial \theta_{xt}}{\partial y}(Q_5 + S_5) + w_b(-T_1) + w_t(T_1),\end{aligned} \tag{15}$$

where the coefficients are defined in Appendix A. The newly defined transverse normal strain can now be written as

$$\begin{aligned}&\varepsilon_{zz}^{(k)} = \bar{u}_{\alpha\beta,x}\lambda_{x\alpha\beta}^{(k)} + \bar{u}_{\alpha\beta,y}\lambda_{y\alpha\beta}^{(k)} + w_\beta\chi_\beta, \\ &\alpha = 1,\ldots,4;\ \beta = 1,2,\end{aligned} \tag{16}$$

where the functions $\lambda_{x\alpha\beta}^{(k)}$, $\lambda_{y\alpha\beta}$ and χ_β are defined in the Appendix A.

The equations of motion, the essential and natural boundary conditions, as well as the displacement-based finite element model can be developed from Hamilton's principle. Again, attention will be limited to a single sublaminate. The energy functional is modified here to include the imposition of the constraints (9) via the penalty method. Hamilton's principle for the mth sublaminate can be defined as follows:

$$\delta\int_{t_0}^{t_1}\{U - K - W + P\}\,\mathrm{d}t = 0. \tag{17}$$

U is the internal strain energy

$$\begin{aligned}U = \sum_{k=1}^{N_m}\int_{V_k}\frac{1}{2}\Big[&\sigma_{xx}^{(k)}\varepsilon_{xx}^{(k)} + \sigma_{yy}^{(k)}\varepsilon_{yy}^{(k)} + \sigma_{zz}^{(k)}\varepsilon_{zz}^{(k)} + \sigma_{yz}^{(k)}\gamma_{yz}^{(k)} \\ &+ \sigma_{zx}^{(k)}\gamma_{zx}^{(k)} + \sigma_{xy}^{(k)}\gamma_{xy}^{(k)}\Big]\,\mathrm{d}V_k,\end{aligned} \tag{18}$$

where V_k is the volume of the kth layer. K is the kinetic energy

$$K = \sum_{k=1}^{N_m}\int_{V_k}\frac{1}{2}\rho^{(k)}\left[\dot{u}_x^{(k)^2} + \dot{u}_y^{(k)^2} + \dot{u}_z^{(k)^2}\right]\mathrm{d}V_k, \tag{19}$$

where $\rho^{(k)}$ is the density of the kth layer and a superposed dot indicates differentiation with respect to time. W is the work of external forces

$$W = \int_\Omega w_\alpha P_\alpha\,\mathrm{d}\Omega + \int_\Gamma t_i u_i\,\mathrm{d}\Gamma, \tag{20}$$

P_α = concentrated forces, $t_i = \sigma_{ij}n_j$,
$\alpha = 1,2,\ i = 1,2.$

P is the penalty constraint

$$\begin{aligned}P = \frac{\gamma}{2}\int_\Omega\Bigg[\sum_{\beta=1}^{2}\Bigg\{&\left(u_{3\beta} - \frac{\partial w_\beta}{\partial y}\right)^2 \\ &+ \left(u_{4\beta} + \frac{\partial w_\beta}{\partial x}\right)^2\Bigg\}\Bigg]\,\mathrm{d}\Omega,\end{aligned} \tag{21}$$

where γ is the penalty parameter. As γ is assigned successively larger values, the constraints of Eq. (9) are satisfied more exactly in the least squares sense. In the internal strain energy expression, Eq. (18), the transverse

normal stress terms require special attention. The constant transverse normal stress leads to an asymmetric stiffness matrix. Thus, σ_{zz} from the constitutive equations, Eq. (2), instead of the constant transverse normal stress, should be employed. Substituting Eqs. (10), (12), (16), (18)–(21) into Eq. (17), taking the variation of Eq. (17), and integrating by parts, Eq. (17) can be rewritten as

$$
\begin{aligned}
&\int_{t_0}^{t_1}\Bigg[\int_{\Omega}\Bigg(\delta\bar{u}_{\alpha\beta}\Bigg\{-\frac{\partial N_{x\alpha\beta}}{\partial x}-\frac{\partial N_{y\alpha\beta}}{\partial y}-\frac{\partial N_{z\alpha\beta}}{\partial x}-\frac{\partial Q_{z\alpha\beta}}{\partial y}\\
&+Q_{y\alpha\beta}+Q_{x\alpha\beta}-\frac{\partial R_{xy\alpha\beta}}{\partial y}-\frac{\partial R_{yx\alpha\beta}}{\partial x}-\gamma\left(\bar{u}_{\alpha\beta}-\frac{\partial w_\beta}{\partial y}\right)\delta_{3\alpha}\\
&-\gamma\left(\bar{u}_{\alpha\beta}+\frac{\partial w_\beta}{\partial x}\right)\delta_{4\alpha}+\frac{\partial^2\bar{u}_{rp}}{\partial t^2}I^u_{\alpha\beta rp}+\frac{\partial^2\bar{u}_{rp}}{\partial t^2}I^v_{\alpha\beta rp}\Bigg\}\\
&+\delta w_\beta\Bigg\{R_{z\beta}-\frac{\partial R_{y\beta}}{\partial y}-\frac{\partial R_{x\beta}}{\partial x}-P_\beta-\gamma\left(\frac{\partial\bar{u}_{3\beta}}{\partial y}-\frac{\partial^2 w_\beta}{\partial y^2}\right)\\
&+\gamma\left(\frac{\partial\bar{u}_{4\beta}}{\partial x}-\frac{\partial^2 w_\beta}{\partial x^2}\right)+\frac{\partial^2 w_p}{\partial t^2}I^w_{\beta p}\Bigg\}\Bigg)\mathrm{d}\Omega\\
&+\oint_s\Bigg(\delta\bar{u}_{\alpha\beta}\{N_{x\alpha\beta}n_x+N_{y\alpha\beta}n_y+N_{z\alpha\beta}n_x+Q_{z\alpha\beta}n_y\\
&+R_{xy\alpha\beta}n_y+R_{yx\alpha\beta}n_x\}+\delta w_\beta\Bigg\{R_{y\beta}n_y\\
&+R_{x\beta}n_x+\gamma n_y\left(\bar{u}_{3\beta}-\frac{\partial w_\beta}{\partial y}\right)-\gamma n_x\left(\bar{u}_{4\beta}+\frac{\partial w_\beta}{\partial x}\right)\Bigg\}\Bigg)\mathrm{d}s\\
&+\int_s\sum_{k=1}^{N_m}\int_{z_{k-1}}^{z_k}\Big(\sigma^{(k)}_{1j}n_j\delta\bar{u}_{\alpha\beta}\Phi^{(k)}_{\alpha\beta}\\
&+\sigma^{(k)}_{2j}n_j\delta\bar{u}_{\alpha\beta}\Psi^{(k)}_{\alpha\beta}\Big)\mathrm{d}z\,\mathrm{d}s\Bigg]\mathrm{d}t=0
\end{aligned}
$$

$$(\alpha,r=1,\ldots,4;\ \beta,p=1,2), \tag{22}$$

where $N_{x\alpha\beta}$, $N_{y\alpha\beta}$, $N_{z\alpha\beta}$, $Q_{z\alpha\beta}$, $Q_{y\alpha\beta}$, $Q_{x\alpha\beta}$, $R_{xy\alpha\beta}$, $R_{yx\alpha\beta}$, $R_{z\beta}$, $R_{y\beta}$, $R_{x\beta}$ are the sublaminate stress resultants shown in the Appendix A, n_x, n_y the directional cosines, $I^u_{\alpha\beta rp}$, $I^v_{\alpha\beta rp}$, $I^w_{\beta p}$, the plate inertias defined in the Appendix A, and $\delta_{\alpha\beta}$ is the Kronecker delta. Considering that variations of the generalized displacement degrees of freedom are independent for $t_0 < t < t_1$ and zero for $t = t_0, t_1$, the equations of motions are derived as

$$
\begin{aligned}
\delta\bar{u}_{\alpha\beta}:\quad &\frac{\partial N_{x\alpha\beta}}{\partial x}+\frac{\partial N_{y\alpha\beta}}{\partial y}+\frac{\partial N_{z\alpha\beta}}{\partial x}+\frac{\partial Q_{z\alpha\beta}}{\partial y}\\
&-Q_{y\alpha\beta}-Q_{x\alpha\beta}+\frac{\partial R_{xy\alpha\beta}}{\partial y}+\frac{\partial R_{yx\alpha\beta}}{\partial x}\\
&+\gamma\left(\bar{u}_{\alpha\beta}-\frac{\partial w_\beta}{\partial y}\right)\delta_{3\alpha}+\gamma\left(\bar{u}_{\alpha\beta}+\frac{\partial w_\beta}{\partial x}\right)\delta_{4\alpha}\\
&=\frac{\partial^2\bar{u}_{rp}}{\partial t^2}I^u_{\alpha\beta rp}+\frac{\partial^2\bar{u}_{rp}}{\partial t^2}I^v_{\alpha\beta rp},\\
\delta w_\beta:\quad &\frac{\partial R_{y\beta}}{\partial y}+\frac{\partial R_{x\beta}}{\partial x}-R_{z\beta}+P_\beta+\gamma\left(\frac{\partial\bar{u}_{3\beta}}{\partial y}-\frac{\partial^2 w_\beta}{\partial y^2}\right)\\
&-\gamma\left(\frac{\partial\bar{u}_{4\beta}}{\partial x}+\frac{\partial^2 w_\beta}{\partial x^2}\right)=\frac{\partial^2 w_p}{\partial t^2}I^w_{\beta p}.
\end{aligned}
\tag{23}
$$

The corresponding boundary conditions are

Essential BC Natural BC

$$
\begin{aligned}
\bar{u}_{\alpha\beta}:\quad &(N_{x\alpha\beta}n_x+N_{y\alpha\beta}n_y+N_{z\alpha\beta}n_x+Q_{z\alpha\beta}n_y\\
&+R_{xy\alpha\beta}n_y+R_{yx\alpha\beta}n_x)\\
&+\sum_{k=1}^{N_m}\int_{z_{k-1}}^{z_k}\Big(\sigma^{(k)}_{1j}n_j\Phi^{(k)}_{\alpha\beta}+\sigma^{(k)}_{2j}n_j\Psi^{(k)}_{\alpha\beta}\Big)\mathrm{d}z,\\
w_\beta:\quad &R_{y\beta}n_y+R_{x\beta}n_x+\gamma n_y\left(\bar{u}_{3\beta}-\frac{\partial w_\beta}{\partial y}\right)\\
&-\gamma n_x\left(\bar{u}_{4\beta}+\frac{\partial w_\beta}{\partial x}\right).
\end{aligned}
\tag{24}
$$

3. Finite element formulation

Since the primary variables are functions of x, y and t only in Eq. (22), we need to consider only two-dimensional shape functions for the finite element model. The most obvious element to be developed would be a simple four-noded plate element with 10 degrees of freedom per node (five bottom surface d.o.f + five top surface d.o.f). However, such an element would not fall within the constraints of having three translational and three rotational degrees of freedom per node. (Most available commercial codes do not allow more than six d.o.f per node.) Even more importantly, a major advantage of the present formulation would be lost if a traditional four-noded element were developed. Because the degrees of freedom represent quantities at the surfaces of a sublaminate (this was not by chance), it is most reasonable to develop the finite element model in the form of an eight-noded element with five degrees of freedom per node

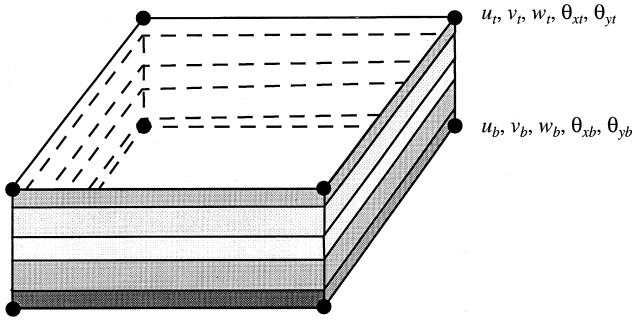

Fig. 3. Element topology and nodal degrees of freedom.

(see Fig. 3). Such elements are classified here as "regenerated," in contrast to the popular "degenerated" shell elements obtained by imposing constraints on solid elements. This approach has been used with great success [22,23], and has the very important advantage of allowing discretization in both in-plane and through-thickness directions without the need for any special multi-point constraints. Elements are assembled in the standard way. Therefore, the element can be used to predict the global response of a laminate using only one (or a small number) of elements through-the-thickness, and local effects such as interlaminar stresses can be captured by refining the mesh in the thickness direction near the interface(s) of interest. The capability of discretization in the through-thickness direction also enables one to simulate the separation of laminated composites due to delamination.

In-plane displacement and rotational degrees of freedom are approximated by the bilinear Lagrange interpolation functions:

$$\begin{aligned} \bar{u}_{1\beta} &= \sum_{i=1}^{4} u_{\beta i} P_i, \quad \bar{u}_{2\beta} = \sum_{i=1}^{4} v_{\beta i} P_i, \\ \bar{u}_{3\beta} &= \sum_{i=1}^{4} \theta_{x\beta i} P_i, \quad \bar{u}_{4\beta} = \sum_{i=1}^{4} \theta_{y\beta i} P_i, \end{aligned} \tag{25}$$

where

$$P_i = \frac{1}{4}(1+\xi_i\xi)(1+\eta_i\eta) \tag{26}$$

and ξ, η are the element natural (local) coordinates. For transverse deflection degrees of freedom, an interdependent interpolation concept similar to that developed by Tessler and Hughes [25] is utilized (see [23] for details) as follows:

$$w = \sum_{i=1}^{4} (P_i w_i + N_{xi}\theta_{xi} + N_{yi}\theta_{yi}), \tag{27}$$

where N_{xi} and N_{yi} depend on N_{i+4} and the projections of each edge onto x and y axes:

$$\begin{aligned} N_{x1} &= -\frac{1}{8}(y_{12}N_5 - y_{41}N_8), \\ N_{y1} &= \frac{1}{8}(x_{12}N_5 - x_{41}N_8), \\ N_{x2} &= -\frac{1}{8}(y_{23}N_6 - y_{12}N_5), \\ N_{y2} &= \frac{1}{8}(x_{23}N_6 - x_{12}N_5), \\ N_{x3} &= -\frac{1}{8}(y_{34}N_7 - y_{23}N_6), \\ N_{y3} &= \frac{1}{8}(x_{34}N_7 - x_{23}N_6), \\ N_{x4} &= -\frac{1}{8}(y_{41}N_8 - y_{34}N_7), \\ N_{y4} &= \frac{1}{8}(x_{41}N_8 - x_{34}N_7), \end{aligned} \tag{28}$$

where

$$\begin{aligned} N_5 &= \frac{1}{2}(1-\xi^2)(1-\eta), \\ N_6 &= \frac{1}{2}(1-\eta^2)(1+\xi), \\ N_7 &= \frac{1}{2}(1-\xi^2)(1+\eta), \\ N_8 &= \frac{1}{2}(1-\eta^2)(1-\xi), \\ x_{ij} &= x_i - x_j, \quad y_{ij} = y_i - y_j. \end{aligned} \tag{29}$$

The interdependent interpolation scheme alleviates the shear locking problem but does not eliminate it totally. The element developed using this scheme still locks in the very thin regime. Prathap and Somashekar found that the source of the shear locking phenomenon comes from inconsistency of the transverse shear strain fields with respect to the in-plane coordinates, x and y [23,26]. Thus, in order to prevent the shear locking phenomenon, we need to make the transverse shear strain fields field consistent. This is performed using the approach presented in [26] (see also [23]).

Even with the choice of field-consistent transverse shear strain fields, the element still locks if edge-consistency of transverse shear strains on any common inter-element edge is not met, especially for general quadrilateral elements. It is crucial to ensure matching of the tangential shear strain on any common inter-element edge. Mismatch of tangential shear strain will give rise to spurious constraints on the edges when the shape of elements are general quadrilaterals. This stems from the fact that when the field consistent covariant transverse shear strain is mapped back into global cartesian coordinates from the covariant frame, jacobian transformations of two adjoining elements at their own integration

points will redefine this consistency, and cause a mismatch of tangential shear strain at the common edge. Thus, the choice of sampling points of the jacobian transformations plays a very important role in edge consistency of tangential shear strain at the common edge. Prathap and Somashekar [26] showed that the consistency of tangential shear strain along a common edge between two elements is maintained by transforming field consistent shear strains in the covariant frame into global cartesian fields at each node of the element instead of at Gauss integration points. In this way, edge consistency in the field consistent covariant penalty constraint fields can be treated as well. The consistent definitions of the shear strain fields and the penalty constraint will eliminate locking problems due to spurious constraints and an exact numerical integration rule can be used to evaluate all components of the shear strain energy.

4. Numerical results

The accuracy of the proposed laminated plate theory and the appropriateness of the finite element model were assessed by simulating the response of two different simply supported laminated plates subjected to a transverse double sinusoidal loading as shown in Fig. 4. The elasticity solution of Burton and Noor [27] and the predictions based on the first-order shear deformation theory (FSDT) [7] were used to provide comparison with the current plate results (FZZ3D). For a given location in the plane of the plate, explicit expressions for the through-thickness variation of stresses are provided by the present model. In the plane of the plate, stresses were evaluated at the centroid of each element, where stress is super-convergent [28]. The bending stresses presented in the forthcoming discussion were evaluated at the center of the element that is nearest to the center

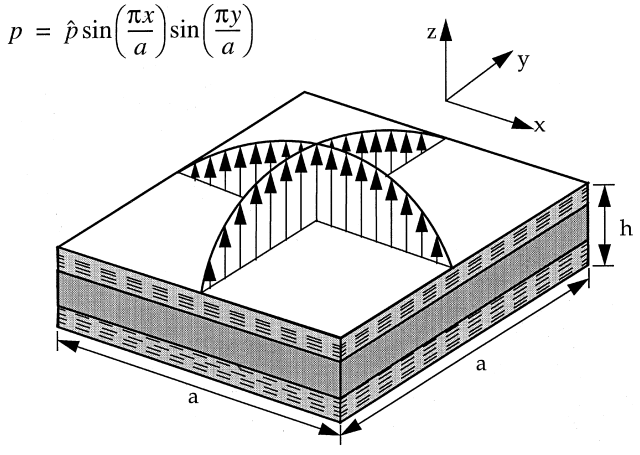

Fig. 4. Simply supported laminated composite plate subjected to sinusoidal loading.

of the plate. The transverse deflections are obtained at the top surface of the center of the plate where load is applied. The in-plane displacements are obtained at the edges of the plate where $x=0$ and $y=a/2$ (for u_β displacement) or $y=0$ and $x=a/2$ (for v_β displacement), and a is the length of each side of the plate. Due to the symmetry of the panels, only a quarter of the plate was modeled in each case. A uniform mesh of 8×8 elements was utilized in the plane of a quarter of the plate, and the through-thickness discretization was varied to assess the utility of the present models. A length-to-thickness aspect ratio of four was chosen in the present examples in order to highlight the ability of the present model to obtain accurate results for very thick laminates via through-thickness refinement of the mesh.

4.1. Example 1: CAV panel

The first example is a panel similar to the US Army TACOM's Composite Armored Vehicle (CAV). Material properties used in the analysis are given in Table 1. The laminate consists of 55 layers and is 4.3 cm (1.7 in.) thick. The laminate can be divided into three sections, as described below:

- *Inner shell*: Four plies of S-2 Glass/Phenolic fabric with stacking sequence $\{[90_2/0_2]\}$ (ply thickness $= 2.54\times10^{-4}$ m (0.01 in.)). Thirty-seven plies of S-2 Glass/8553-40 Epoxy tows with stacking sequence $\{[0/90]$, $[45/-45/0/90]_4$, $[45/0/45]$, $[90/0/-45/45]_4\}$ (ply thickness $= 5.334\times10^{-4}$ m (0.021 in.)).
- *Armor core*: One layer of EPDM rubber (ply thickness $= 1.778\times10^{-3}$ m (0.0625 in.)) and one layer of ceramic tile with inserts (ply thickness $= 1.778\times10^{-2}$ m (0.7 in.)).
- *Outer shell*: Twelve plies of S-2 Glass/8553-40 Epoxy fabric with stacking sequence $[0/90/45/-45/0/90]_s$ (ply thickness $= 2.54\times10^{-4}$ m (0.01 in.)).

To allow comparison of predictions of the current model with the elasticity solution, all layers are oriented at either 90° or 0° from the reference axis by replacing all 45° plies with 90° plies and −45° plies with 0° plies. Two types of through-thickness refinement were used in the analyses: (1) a single sublaminate, and (2) three sublaminates with a sublaminate for the inner shell, a sublaminate for the rubber layer, and a sublaminate for the ceramic tile layer and the outer shell.

The influence of aspect ratios on transverse deflection is shown in Fig. 5. Eight different aspect ratios were considered to check a wide range of plate bending behavior ($a/h=4$, 8, 10, 20, 30, 50, 100, 500, and 1000). When one sublaminate was used, the error in predicted deflection was about 15% for the case $a/h=4$. The use of three sublaminates resulted in more accurate predictions, with an error of less than 1%. It was observed that the prediction of transverse deflection converges rapidly

Table 1
Material properties for TACOM's composite armored vehicle (CAV) panel

	S-2 Glass/Phenolic Fabric	S-2 Glass/8553-40 Tow	S-2 Glass/8553-40 Fabric	EPDM Rubber	Ceramic
E_{11} (GPa)	20.7	42.7	20.7	0.021	34.5
E_{22} (GPa)	20.7	6.9	20.7	0.021	34.5
E_{33} (GPa)	8.27	6.9	7.58	0.021	0.86
v_{12}	0.13	0.29	0.13	0.45	0.15
v_{23}	0.18	0.37	0.18	0.45	0.15
v_{13}	0.18	0.29	0.18	0.45	0.15
G_{12} (GPa)	6.9	2.07	6.9	0.0069	17.24
G_{23} (GPa)	3.17	2.07	2.69	0.0069	0.059
G_{13} (GPa)	3.17	2.07	2.69	0.0069	0.059

to the exact solution as more sublaminates are used. In Fig. 6, the variation of in-plane displacement, u_x, through-the-thickness of the laminate is plotted at $x=0$ and $y=a/2$ for an aspect ratio of four. The exact distribution of in-plane displacement is approximately linear within each layer, and globally piece-wise linear and of zig-zag pattern due to the difference in the shear moduli of adjacent layers. It is shown that the current model containing only one sublaminate captures the trends of the distribution of displacement very well,

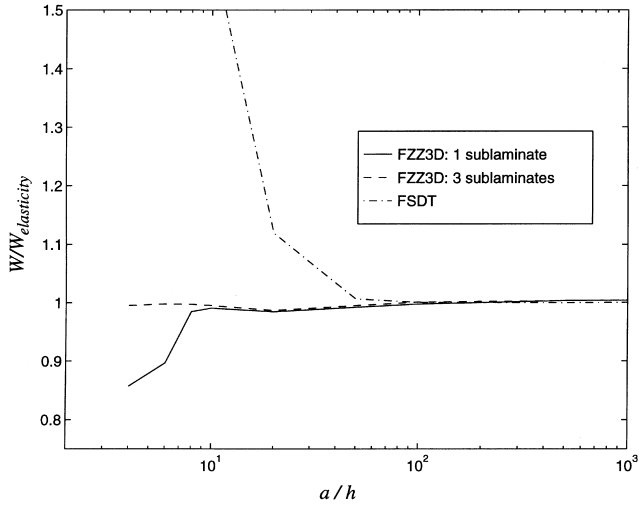

Fig. 5. Variation of normalized center deflection versus plate aspect ratio at the center of the plate (CAV panel).

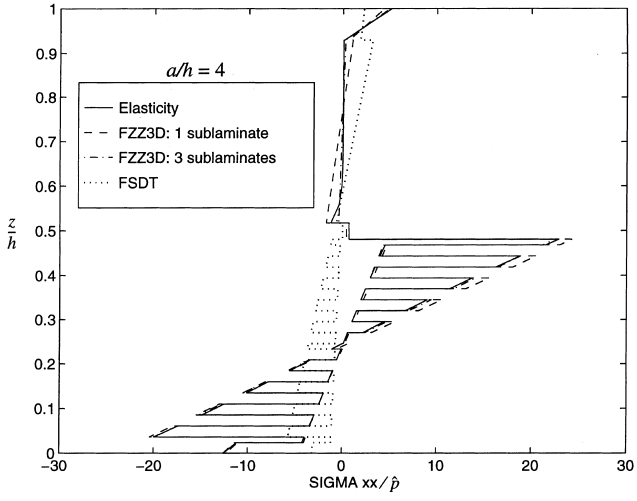

Fig. 7. Normalized bending stress, σ_{xx}, versus normalized thickness coordinate at the center of the plate (CAV panel, $a/h=4$).

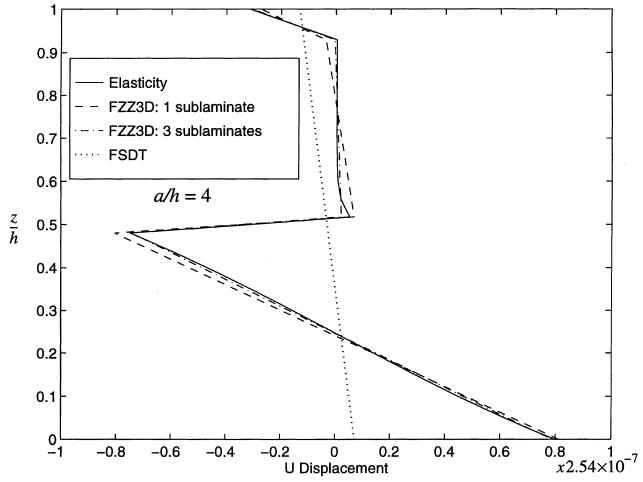

Fig. 6. In-plane displacement, u, versus normalized thickness coordinate (CAV panel, $a/h=4$).

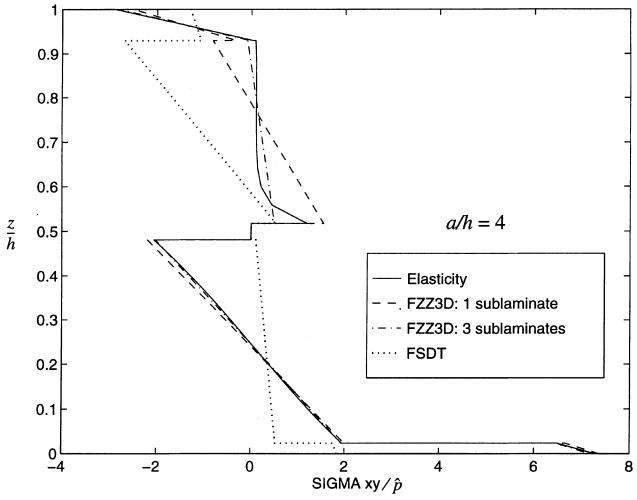

Fig. 8. Normalized in-plane shear stress, σ_{xy}, versus normalized thickness coordinate at $x,y=0$, (CAV panel, $a/h=4$).

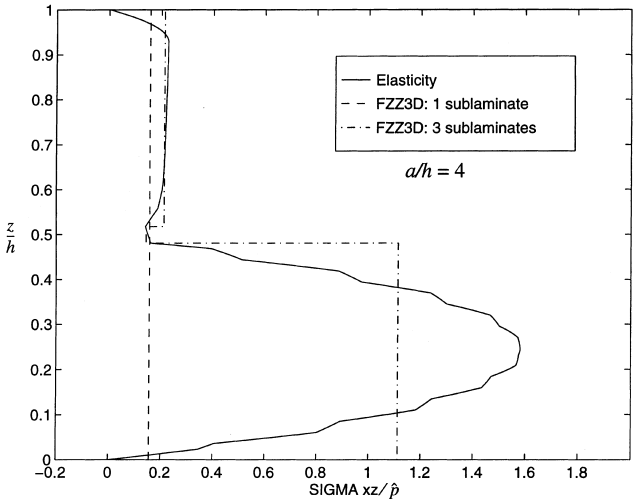

Fig. 9. Normalized transverse shear stress, σ_{xz}, versus normalized thickness coordinate at $x=0$, $y=2/a$ (CAV panel, $a/h=4$).

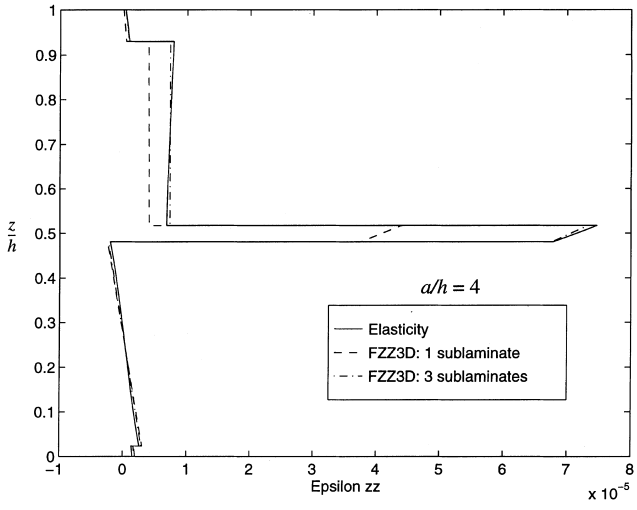

Fig. 10. Transverse normal strain, ε_{zz}, versus normalized thickness coordinate at the center of the plate (CAV panel, $a/h=4$).

while FSDT is unable to simulate such behavior. The bending stress distribution through-the-thickness is illustrated in Fig. 7. The stress was evaluated at the Gauss point nearest to the center of the plate. It can be observed that the prediction of in-plane normal stress by the current model agrees well with the elasticity solution. The prediction of in-plane shear stress is shown in Fig. 8. There is significant error in the armor core region, but predictions of the current model are very good in other regions of the laminate. The distribution of transverse shear stress, σ_{xz}, through-the-thickness is shown in Fig. 9. As assumed, this component of stress is constant in each sublaminate. It is shown that the use of multiple sublaminates allows the current model to capture the trends of the through-thickness distribution of shear stress, but point-wise accuracy is not achieved.

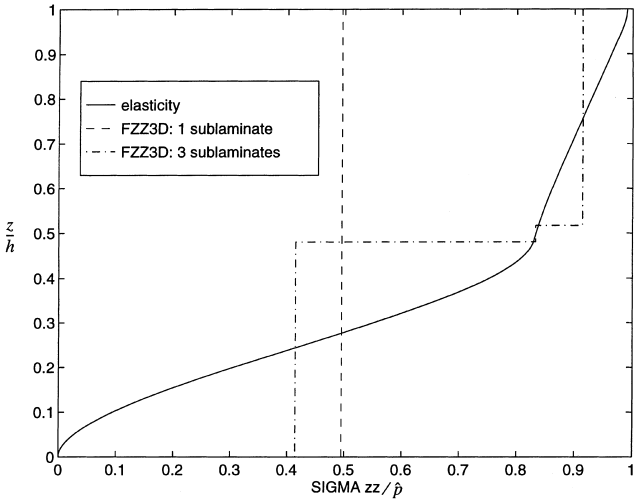

Fig. 11. Normalized transverse normal stress, σ_{zz}, versus normalized thickness coordinate at the center of the plate (CAV panel, $a/h=4$).

The prediction of transverse normal strain, ε_{zz}, is shown in Fig. 10. When three sublaminates are used, the distribution of transverse strain is nearly indistinguishable from the elasticity solution. In Fig. 11, transverse

Table 2
Material properties for sandwich composite plate

	Material 1	Material 2	Material 3	Core
E_{11} (GPa)	6.9	224.8	172.4	0.345
E_{22} (GPa)	172.4	69.0	6.9	1.034
E_{33} (GPa)	6.9	69.0	6.9	0.345
ν_{12}	0.01	0.10	0.25	0.01
ν_{23}	0.25	0.25	0.25	0.15
ν_{13}	0.25	0.10	0.25	0.15
G_{12} (GPa)	3.45	56.6	3.45	0.15
G_{23} (GPa)	3.45	3.45	1.38	0.29
G_{13} (GPa)	1.38	56.6	3.45	0.15

Table 3
Lamination scheme for sandwich panel

Layer no.	Material	Relative thickness
1	1	0.010
2	2	0.025
3	3	0.015
4	1	0.020
5	3	0.030
6	Core	0.800
7	3	0.030
8	1	0.020
9	3	0.015
10	2	0.025
11	1	0.010

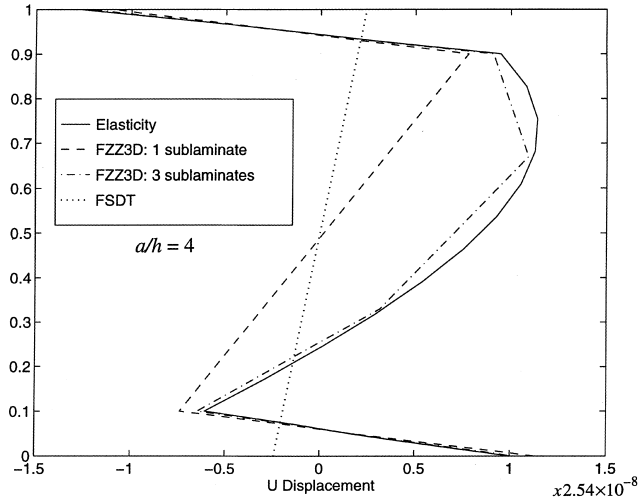

Fig. 12. In-plane displacement, u, versus normalized thickness coordinate (Sandwich panel, $a/h = 4$).

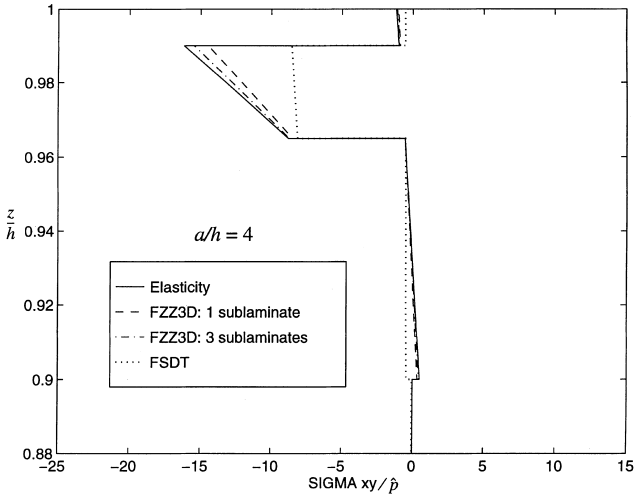

Fig. 14. Normalized in-plane shear stress in the face sheets, σ_{xy}, versus normalized thickness coordinate at $x, y = 0$, (CAV panel, $a/h = 4$).

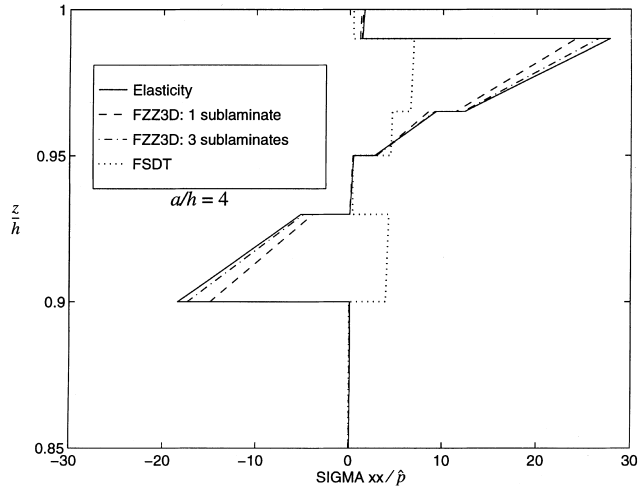

Fig. 13. Normalized bending stress, σ_{xx}, in face sheets versus normalized thickness coordinate (Sandwich plate, $a/h = 4$).

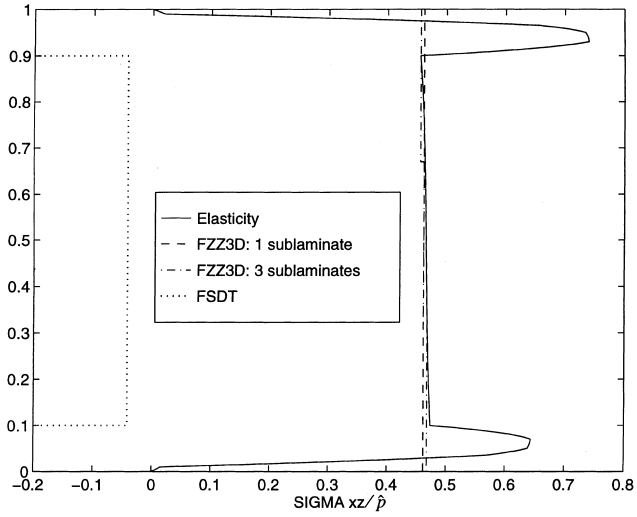

Fig. 15. Normalized transverse shear stress, σ_{xz}, versus normalized thickness coordinate at $x = 0$, $y = 2/i$ (Sandwich panel, $a/h = 4$).

normal stress, σ_{zz}, versus normalized thickness coordinate at the center of the plate is illustrated. As assumed, the model captures about the average value of the exact distribution in a sublaminate.

4.2. Example 2: Sandwich panel

The second example is a sandwich panel which consists of a thick core between two sets of five face sheets. The material properties used in the analysis are listed in Table 2, and the lamination scheme is defined in Table 3. The core occupies 80% of the thickness of the plate, while each set of face sheets contains five layers and occupies 10% of the total thickness. Two types of through-thickness discretization were used in the analyses: (1) a single sublaminate, (2) three sublaminates with equal thickness.

In Fig. 12, the predicted through-thickness distributions of in-plane displacement are illustrated. All predictions were very accurate in the upper and lower face sheet regions, but there were significant errors in the core region when only one sublaminate was used. These errors were due to the very large transverse shear strains and transverse squashing in the core of this thick sandwich plate. The nonlinear variation of in-plane displacement in this region could not be captured accurately by a single sublaminate in the core region. For thinner plates (i.e., a/h greater than about 10), the in-plane displacements through-the-thickness are predicted satisfactorily using a single sublaminate through the

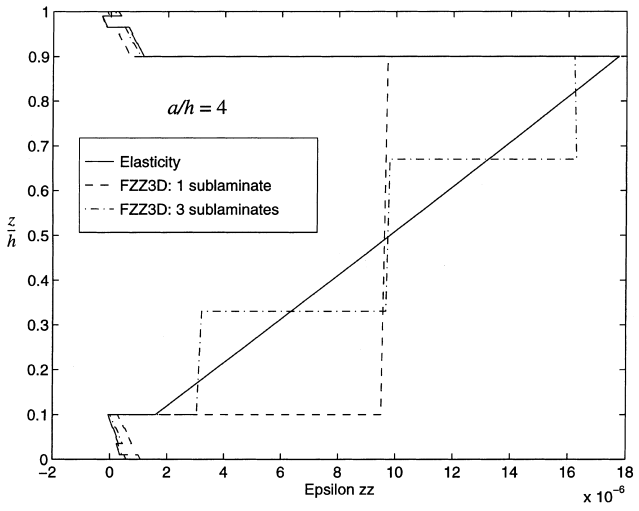

Fig. 16. Transverse normal strain, ϵ_{zz}, versus normalized thickness coordinate at the center of the plate (Sandwich panel, $a/h = 4$).

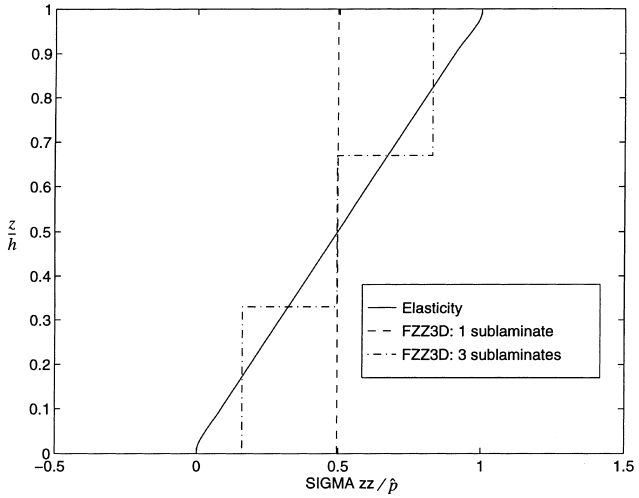

Fig. 17. Normalized transverse normal stress, σ_{zz}, versus normalized thickness coordinate at the center of the plate (Sandwich panel, $a/h = 4$).

entire thickness of the laminate. To assess the bending stress, σ_{xx}, more clearly, the stress distribution in the upper face sheet region is enlarged and shown in Fig. 13. It can be observed that the current finite element model using only one sublaminate predicts the stress distribution in the face sheets fairly accurately, and even greater accuracy is achieved with three sublaminates. In Fig. 14, in-plane shear stress in the face sheets are predicted. It is shown in Fig. 15 that the average transverse shear stress is captured well by the current model. Fig. 16 depicts the distribution of transverse normal strain, ε_{zz}, through-the-thickness of the laminate. When three sublaminates were employed, the strain distribution through-the-thickness is predicted relatively well, capturing the trend in the core region. Predictions of transverse normal stress, σ_{zz}, versus normalized thickness coordinate at the center of the plate are shown in Fig. 17. The model predicts about the average value of the exact distribution in a sublaminate, and captures the distribution trends as more elements are used through-the-thickness.

5. Conclusions

An improved first-order zig-zag theory and an associated finite element model were presented. The model allows the representation of a laminate as an assemblage of sublaminates in order to increase the model refinement through-the-thickness, when needed. Within each sublaminate, an accurate first-order zig-zag sublaminate kinematic approximation is made which minimizes the need for multiple sublaminates for many problems of practical interest yet easily accommodates through-thickness refinement for predicting local variations of stress and deformation. The finite element model is 'regenerated' in the form of an eight-noded three-dimensional element with five degrees of freedom (three translations and two rotations) per node. Thus, it is suitable for implementation into commercial finite element codes. Numerical results demonstrate that the current model is accurate, efficient, and robust for analysis of a wide variety of thick or thin laminated plates.

Acknowledgements

This work was partially supported by NASA Langley Research Center under Grant NAG-1-1591. This support and the helpful comments of Alex Tessler, grant monitor, are gratefully acknowledged.

Appendix A

A.1. Shape functions

The rotational variables ψ_x and ψ_y are eliminated in favor of the translational variables u_t and v_t, the in-plane translations at the top surface of the sublaminate. In that process the following variables are obtained:

$$A = h + \sum_{i=1}^{N_m}(h - z_i)d_i, \quad B = \sum_{i=1}^{N_m}(h - z_i)c_i,$$
$$C = \sum_{i=1}^{N_m}(h - z_i)b_i, \quad D = h + \sum_{i=1}^{N_m}(h - z_i)a_i, \tag{A.1}$$
$$\bar{\Delta} = A \cdot D - B \cdot C,$$

where h is the thickness of mth sublaminate, and a_i, b_i, c_i, d_i are defined in Eq. (7).

$$\alpha_1 = \frac{D}{\bar{\Delta}}, \quad \alpha_2 = -\frac{B}{\bar{\Delta}},$$
$$\alpha_3 = \frac{\{B \cdot C - D \cdot (A - h)\}}{2\bar{\Delta}}, \quad \alpha_4 = \frac{-B \cdot h}{2,}$$
$$\beta_1 = -\frac{C}{\bar{\Delta}}, \quad \beta_2 = \frac{A}{\bar{\Delta}}, \quad \beta_3 = -\frac{C \cdot h}{2\bar{\Delta}},$$
$$\beta_4 = \frac{\{B \cdot C - A \cdot (D - h)\}}{2\bar{\Delta}} \tag{A.2}$$

$$\bar{A}_1 = \alpha_1 + \beta_1 \sum_{i=1}^{k-1} c_i + \alpha_1 \sum_{i=1}^{k-1} d_i,$$
$$\bar{A}_2 = \beta_1 \sum_{i=1}^{k-1} c_i z_i + \alpha_1 \sum_{i=1}^{k-1} d_i z_i,$$
$$\bar{B}_1 = \alpha_2 + \beta_2 \sum_{i=1}^{k-1} c_i + \alpha_2 \sum_{i=1}^{k-1} d_i,$$
$$\bar{B}_2 = \beta_2 \sum_{i=1}^{k-1} c_i z_i + \alpha_2 \sum_{i=1}^{k-1} d_i z_i,$$
$$\bar{C}_1 = \alpha_3 + \beta_3 \sum_{i=1}^{k-1} c_i + \left(\alpha_3 + \frac{1}{2}\right) \sum_{i=1}^{k-1} d_i,$$
$$\bar{C}_2 = \beta_3 \sum_{i=1}^{k-1} c_i z_i + \left(\alpha_3 + \frac{1}{2}\right) \sum_{i=1}^{k-1} d_i z_i,$$
$$\bar{D}_1 = \alpha_4 + \left(\beta_4 + \frac{1}{2}\right) \sum_{i=1}^{k-1} c_i + \alpha_4 \sum_{i=1}^{k-1} d_i,$$
$$\bar{D}_2 = \left(\beta_4 + \frac{1}{2}\right) \sum_{i=1}^{k-1} c_i z_i + \alpha_4 \sum_{i=1}^{k-1} d_i z_i,$$
$$\hat{A}_1 = \beta_1 + \beta_1 \sum_{i=1}^{k-1} a_i + \alpha_1 \sum_{i=1}^{k-1} b_i,$$
$$\hat{A}_2 = \beta_1 \sum_{i=1}^{k-1} a_i z_i + \alpha_1 \sum_{i=1}^{k-1} b_i z_i,$$
$$\hat{B}_1 = \beta_2 + \beta_2 \sum_{i=1}^{k-1} a_i + \alpha_2 \sum_{i=1}^{k-1} b_i,$$
$$\hat{B}_2 = \beta_2 \sum_{i=1}^{k-1} a_i z_i + \alpha_2 \sum_{i=1}^{k-1} b_i z_i,$$
$$\hat{C}_1 = \beta_3 + \beta_3 \sum_{i=1}^{k-1} a_i + \left(\alpha_3 + \frac{1}{2}\right) \sum_{i=1}^{k-1} b_i,$$
$$\hat{C}_2 = \beta_3 \sum_{i=1}^{k-1} a_i z_i + \left(\alpha_3 + \frac{1}{2}\right) \sum_{i=1}^{k-1} b_i z_i,$$
$$\hat{D}_1 = \beta_4 + \left(\beta_4 + \frac{1}{2}\right) \sum_{i=1}^{k-1} a_i + \alpha_4 \sum_{i=1}^{k-1} b_i,$$
$$\hat{D}_2 = \left(\beta_4 + \frac{1}{2}\right) \sum_{i=1}^{k-1} a_i z_i + \alpha_4 \sum_{i=1}^{k-1} b_i z_i. \tag{A.3}$$

The shape functions for $u_x^{(k)}$ are

$$\Phi_{11}^{(k)} = -\bar{A}_1 z + 1 + \bar{A}_2, \quad \Phi_{12}^{(k)} = \bar{A}_1 z - \bar{A}_2,$$
$$\Phi_{21}^{(k)} = -\bar{B}_1 z + \bar{B}_2, \quad \Phi_{22}^{(k)} = \bar{B}_1 z - \bar{B}_2,$$
$$\Phi_{31}^{(k)} = \Phi_{32}^{(k)} = \bar{D}_1 z - \bar{D}_2,$$
$$\Phi_{41}^{(k)} = \Phi_{42}^{(k)} = -\bar{C}_1 z + \bar{C}_2. \tag{A.4}$$

The shape functions for $u_y^{(k)}$ are

$$\Psi_{11}^{(k)} = -\hat{A}_1 z + \hat{A}_2, \quad \Psi_{12}^{(k)} = \hat{A}_1 z - \hat{A}_2,$$
$$\Psi_{21}^{(k)} = -\hat{B}_1 z + \hat{B}_2 + 1, \quad \Psi_{22}^{(k)} = \hat{B}_1 z - \hat{B}_2,$$
$$\Psi_{31}^{(k)} = \Psi_{32}^{(k)} = \hat{D}_1 z - \hat{D}_2,$$
$$\Psi_{41}^{(k)} = \Psi_{42}^{(k)} = -\hat{C}_1 z + \hat{C}_2. \tag{A.5}$$

The shape functions for $u_z^{(k)}$ are

$$\Omega_1 = 1 - \frac{z}{h}, \quad \Omega_2 = \frac{z}{h}. \tag{A.6}$$

The shape functions associated with ε_{zz} based on a constant transverse normal stress assumption are

$$\lambda_{x11}^{(k)} = \bar{E}_1 z + \bar{E}_2, \quad \lambda_{x12}^{(k)} = \bar{F}_1 z + \bar{F}_2,$$
$$\lambda_{x21}^{(k)} = \bar{G}_1 z + \bar{G}_2, \quad \lambda_{x22}^{(k)} = \bar{H}_1 z + \bar{H}_2,$$
$$\lambda_{x31}^{(k)} = \lambda_{x32}^{(k)} = \bar{I}_1 z + \bar{I}_2, \quad \lambda_{x41}^{(k)} = \lambda_{x42}^{(k)} = \bar{J}_1 z + \bar{J}_2,$$
$$\lambda_{y11}^{(k)} = \hat{E}_1 z + \hat{E}_2, \quad \lambda_{y12}^{(k)} = \hat{F}_1 z + \hat{F}_2,$$
$$\lambda_{y21}^{(k)} = \hat{G}_1 z + \hat{G}_2, \quad \lambda_{y22}^{(k)} = \hat{H}_1 z + \hat{H}_2,$$
$$\lambda_{y31}^{(k)} = \lambda_{y32}^{(k)} = \hat{I}_1 z + \hat{I}_2, \quad \lambda_{y41}^{(k)} = \lambda_{y42}^{(k)} = \hat{J}_1 z + \hat{J}_2,$$
$$\chi_1 = -K_1, \quad \chi_2 = K_1, \tag{A.7}$$

where coefficients associated with the shape functions are

$$\bar{E}_1 = \frac{C_{13}^{(k)}}{C_{33}^{(k)}} \bar{A}_1 + \frac{C_{36}^{(k)}}{C_{33}^{(k)}} \hat{A}_1,$$
$$\bar{E}_2 = -\frac{C_{13}^{(k)}}{C_{33}^{(k)}} (\bar{A}_2 + 1) - \frac{C_{36}^{(k)}}{C_{33}^{(k)}} \hat{A}_2 + \frac{P_1 + S_6}{C_{33}^{(k)}},$$
$$\bar{F}_1 = -\frac{C_{13}^{(k)}}{C_{33}^{(k)}} \bar{A}_1 - \frac{C_{36}^{(k)}}{C_{33}^{(k)}} \hat{A}_1,$$
$$\bar{F}_2 = \frac{C_{13}^{(k)}}{C_{33}^{(k)}} \bar{A}_2 + \frac{C_{36}^{(k)}}{C_{33}^{(k)}} \hat{A}_2 + \frac{P_2 - S_6}{C_{33}^{(k)}},$$
$$\bar{G}_1 = \frac{C_{13}^{(k)}}{C_{33}^{(k)}} \bar{B}_1 + \frac{C_{36}^{(k)}}{C_{33}^{(k)}} \hat{B}_1,$$
$$\bar{G}_2 = -\frac{C_{13}^{(k)}}{C_{33}^{(k)}} \bar{B}_2 - \frac{C_{36}^{(k)}}{C_{33}^{(k)}} (\hat{B}_2 + 1) + \frac{P_3 + S_7}{C_{33}^{(k)}},$$

$$\bar{H}_1 = -\frac{C_{13}^{(k)}}{C_{33}^{(k)}}\bar{B}_1 - \frac{C_{36}^{(k)}}{C_{33}^{(k)}}\hat{B}_1,$$

$$\bar{H}_2 = \frac{C_{13}^{(k)}}{C_{33}^{(k)}}\bar{B}_2 + \frac{C_{36}^{(k)}}{C_{33}^{(k)}}\hat{B}_2 + \frac{-P_3 + S_8}{C_{33}^{(k)}},$$

$$\bar{I}_1 = \frac{C_{13}^{(k)}}{C_{33}^{(k)}}\bar{C}_1 + \frac{C_{36}^{(k)}}{C_{33}^{(k)}}\hat{C}_1,$$

$$\bar{I}_2 = -\frac{C_{13}^{(k)}}{C_{33}^{(k)}}\bar{C}_2 - \frac{C_{36}^{(k)}}{C_{33}^{(k)}}\hat{C}_2 + \frac{P_4 + S_9}{C_{33}^{(k)}},$$

$$\bar{J}_1 = -\frac{C_{13}^{(k)}}{C_{33}^{(k)}}\bar{D}_1 - \frac{C_{36}^{(k)}}{C_{33}^{(k)}}\hat{D}_1,$$

$$\bar{J}_2 = \frac{C_{13}^{(k)}}{C_{33}^{(k)}}\bar{D}_2 + \frac{C_{36}^{(k)}}{C_{33}^{(k)}}\hat{D}_2 + \frac{P_5 + S_{10}}{C_{33}^{(k)}},$$

$$\hat{E}_1 = \frac{C_{23}^{(k)}}{C_{33}^{(k)}}\hat{A}_1 + \frac{C_{36}^{(k)}}{C_{33}^{(k)}}\bar{A}_1,$$

$$\hat{E}_2 = -\frac{C_{23}^{(k)}}{C_{33}^{(k)}}\hat{A}_2 - \frac{C_{36}^{(k)}}{C_{33}^{(k)}}(\bar{A}_2 + 1) + \frac{Q_1 + S_1}{C_{33}^{(k)}},$$

$$\hat{F}_1 = -\frac{C_{23}^{(k)}}{C_{33}^{(k)}}\hat{A}_1 - \frac{C_{36}^{(k)}}{C_{33}^{(k)}}\bar{A}_1,$$

$$\hat{F}_2 = \frac{C_{23}^{(k)}}{C_{33}^{(k)}}\hat{A}_2 + \frac{C_{36}^{(k)}}{C_{33}^{(k)}}\bar{A}_2 + \frac{-Q_1 + S_2}{C_{33}^{(k)}}, \tag{A.8}$$

$$\hat{G}_1 = \frac{C_{23}^{(k)}}{C_{33}^{(k)}}\hat{B}_1 + \frac{C_{36}^{(k)}}{C_{33}^{(k)}}\bar{B}_1,$$

$$\hat{G}_2 = -\frac{C_{23}^{(k)}}{C_{33}^{(k)}}(\hat{B}_2 + 1) - \frac{C_{36}^{(k)}}{C_{33}^{(k)}}\bar{B}_2 + \frac{Q_2 + S_3}{C_{33}^{(k)}},$$

$$\hat{H}_1 = -\frac{C_{23}^{(k)}}{C_{33}^{(k)}}\hat{B}_1 - \frac{C_{36}^{(k)}}{C_{33}^{(k)}}\bar{B}_1,$$

$$\hat{H}_2 = \frac{C_{23}^{(k)}}{C_{33}^{(k)}}\hat{B}_2 + \frac{C_{36}^{(k)}}{C_{33}^{(k)}}\bar{B}_2 + \frac{Q_3 - S_3}{C_{33}^{(k)}},$$

$$\hat{I}_1 = \frac{C_{23}^{(k)}}{C_{33}^{(k)}}\hat{C}_1 + \frac{C_{36}^{(k)}}{C_{33}^{(k)}}\bar{C}_1,$$

$$\hat{I}_2 = -\frac{C_{23}^{(k)}}{C_{33}^{(k)}}\hat{C}_2 - \frac{C_{36}^{(k)}}{C_{33}^{(k)}}\bar{C}_2 + \frac{Q_4 + S_4}{C_{33}^{(k)}},$$

$$\hat{J}_1 = -\frac{C_{23}^{(k)}}{C_{33}^{(k)}}\hat{D}_1 - \frac{C_{36}^{(k)}}{C_{33}^{(k)}}\bar{D}_1,$$

$$\hat{J}_2 = \frac{C_{23}^{(k)}}{C_{33}^{(k)}}\hat{D}_2 + \frac{C_{36}^{(k)}}{C_{33}^{(k)}}\bar{D}_2 + \frac{Q_5 + S_5}{C_{33}^{(k)}},$$

$$K_1 = \frac{T_1}{C_{33}^{(k)}}.$$

$$P_1 = C_{13}^{(k)}\left\{-\frac{\bar{A}_1}{2}(z_k + z_{k-1}) + (1 + \bar{A}_2)\right\},$$

$$P_2 = C_{13}^{(k)}\left\{\frac{\bar{A}_1}{2}(z_k + z_{k-1}) - \bar{A}_2\right\},$$

$$P_3 = C_{13}^{(k)}\left\{-\frac{\bar{B}_1}{2}(z_k + z_{k-1}) + \bar{B}_2)\right\},$$

$$P_4 = C_{13}^{(k)}\left\{-\frac{\bar{C}_1}{2}(z_k + z_{k-1}) + \bar{C}_2\right\},$$

$$P_5 = C_{13}^{(k)}\left\{\frac{\bar{D}_1}{2}(z_k + z_{k-1}) - \bar{D}_2)\right\},$$

$$Q_1 = C_{23}^{(k)}\left\{-\frac{\hat{A}_1}{2}(z_k + z_{k-1}) + \hat{A}_2\right\},$$

$$Q_2 = C_{23}^{(k)}\left\{-\frac{\hat{B}_1}{2}(z_k + z_{k-1}) + \hat{B}_2 + 1\right\},$$

$$Q_3 = C_{23}^{(k)}\left\{\frac{\hat{B}_1}{2}(z_k + z_{k-1}) - \hat{B}_2\right\},$$

$$Q_4 = C_{23}^{(k)}\left\{-\frac{\hat{C}_1}{2}(z_k + z_{k-1}) + \hat{C}_2\right\},$$

$$Q_5 = C_{23}^{(k)}\left\{\frac{\hat{D}_1}{2}(z_k + z_{k-1}) - \hat{D}_2\right\},$$

$$S_1 = C_{36}^{(k)}\left\{-\frac{\bar{A}_1}{2}(z_k + z_{k-1}) + (1 + \bar{A}_2)\right\}, \tag{A.9}$$

$$S_2 = C_{36}^{(k)}\left\{\frac{\bar{A}_1}{2}(z_k + z_{k-1}) - \bar{A}_2\right\},$$

$$S_3 = C_{36}^{(k)}\left\{-\frac{\bar{B}_1}{2}(z_k + z_{k-1}) + \bar{B}_2\right\},$$

$$S_4 = C_{36}^{(k)}\left\{-\frac{\bar{C}_1}{2}(z_k + z_{k-1}) + \bar{C}_2\right\},$$

$$S_5 = C_{36}^{(k)}\left\{\frac{\bar{D}_1}{2}(z_k + z_{k-1}) - \bar{D}_2\right\},$$

$$S_6 = C_{36}^{(k)}\left\{-\frac{\hat{A}_1}{2}(z_k + z_{k-1}) + \hat{A}_2\right\},$$

$$S_7 = C_{23}^{(k)}\left\{-\frac{\hat{B}_1}{2}(z_k + z_{k-1}) + \hat{B}_2 + 1\right\},$$

$$S_8 = C_{36}^{(k)}\left\{\frac{\hat{B}_1}{2}(z_k + z_{k-1}) - \hat{B}_2\right\},$$

$$S_9 = C_{23}^{(k)}\left\{-\frac{\hat{C}_1}{2}(z_k + z_{k-1}) + \hat{C}_2)\right\},$$

$$S_{10} = C_{23}^{(k)}\left\{\frac{\hat{D}_1}{2}(z_k + z_{k-1}) - \hat{D}_2\right\},$$

$$T_1 = \frac{C_{33}^{(k)}}{h}.$$

A.2. Plate inertias

$$
\begin{aligned}
I^{u}_{\alpha\beta rp} &= \sum_{k=1}^{N_m} \int_{z_{k-1}}^{z_k} \rho^{(k)} \Phi^{(k)}_{\alpha\beta} \Phi^{(k)}_{rp} \, \mathrm{d}z, \\
I^{v}_{\alpha\beta rp} &= \sum_{k=1}^{N_m} \int_{z_{k-1}}^{z_k} \rho^{(k)} \Psi^{(k)}_{\alpha\beta} \Psi^{(k)}_{rp} \, \mathrm{d}z, \\
I^{w}_{p\beta rp} &= \sum_{k=1}^{N_m} \int_{z_{k-1}}^{z_k} \rho^{(k)} \Omega_{\beta} \Omega_{p} \, \mathrm{d}z, \\
&\alpha, r = 1, \ldots, 4, \;\; \beta, p = 1, 2.
\end{aligned}
\tag{A.10}
$$

A.3. Stress resultants

$$
\begin{aligned}
N_{x\alpha\beta} &= \sum_{k=1}^{N_m} \int_{z_{k-1}}^{z_k} \sigma^{(k)}_{xx} \Phi^{(k)}_{\alpha\beta} \, \mathrm{d}z, \quad N_{y\alpha\beta} = \sum_{k=1}^{N_m} \int_{z_{k-1}}^{z_k} \sigma^{(k)}_{yy} \Psi^{(k)}_{\alpha\beta} \, \mathrm{d}z, \\
N_{z\alpha\beta} &= \sum_{k=1}^{N_m} \int_{z_{k-1}}^{z_k} \sigma^{(k)}_{zz} \lambda^{(k)}_{x\alpha\beta} \, \mathrm{d}z, \quad Q_{z\alpha\beta} = \sum_{k=1}^{N_m} \int_{z_{k-1}}^{z_k} \sigma^{(k)}_{zz} \lambda^{(k)}_{y\alpha\beta} \, \mathrm{d}z, \\
R_{z\beta} &= \sum_{k=1}^{N_m} \int_{z_{k-1}}^{z_k} \sigma^{(k)}_{zz} \chi_{\beta} \, \mathrm{d}z, \quad Q_{y\alpha\beta} = \sum_{k=1}^{N_m} \int_{z_{k-1}}^{z_k} \tau^{(k)}_{yz} \Psi^{(k)}_{\alpha\beta,z} \, \mathrm{d}z, \\
R_{y\beta} &= \sum_{k=1}^{N_m} \int_{z_{k-1}}^{z_k} \tau^{(k)}_{yz} \bar{M}_{\beta} \, \mathrm{d}z, \quad Q_{x\alpha\beta} = \sum_{k=1}^{N_m} \int_{z_{k-1}}^{z_k} \tau^{(k)}_{xz} \Phi^{(k)}_{\alpha\beta,z} \, \mathrm{d}z, \\
R_{x\beta} &= \sum_{k=1}^{N_m} \int_{z_{k-1}}^{z_k} \tau^{(k)}_{xz} \bar{M}_{\beta} \, \mathrm{d}z, \quad R_{xy\alpha\beta} = \sum_{k=1}^{N_m} \int_{z_{k-1}}^{z_k} \tau^{(k)}_{xy} \Phi^{(k)}_{\alpha\beta} \, \mathrm{d}z, \\
R_{yx\alpha\beta} &= \sum_{k=1}^{N_m} \int_{z_{k-1}}^{z_k} \tau^{(k)}_{xy} \Psi^{(k)}_{\alpha\beta} \, \mathrm{d}z.
\end{aligned}
\tag{A.11}
$$

References

[1] Kapania RK, Raciti S. Recent advances in analysis of laminated beams and plates – Part I: shear effects and buckling. AIAA J 1989;27:923–34.

[2] Noor AK, Burton WS. Assessment of shear deformable theories for multilayered composite plates. Appl Mech Rev 1989;42:1–12.

[3] Noor AK, Burton WS. Assessment of computational models for multilayered composite shells. Appl Mech Rev 1990;43:67–97.

[4] Noor AK. Mechanics of anisotropic plates and shells – a new look at an old subject. Comput Struct 1992;44:499–514.

[5] Reddy JN. A review of refined theories of laminated composite plate. Shock Vibr Dig 1990;22:3–17.

[6] Jemielita G. On kinematical assumptions of refined theories of plates: a survey. J Appl Mech 1990;57:1088–91.

[7] Yang PC, Norris CH, Stavsky Y. Elastic wave propagation in heterogeneous plates. Int J Sol Struct 1966;2:665–84.

[8] Lo KH, Christensen RM, Wu EM. A high-order theory of plate deformation – Part 2: laminated plates. J Appl Mech 1977;44:669–76.

[9] Reddy JN. A simple higher-order theory for laminated composite plates. J Appl Mech 1984;51:745–52.

[10] Tessler A. A higher-order plate theory with ideal finite element suitability. Comp Meth Appl Mech Eng 1991;85:183–205.

[11] Reddy JN. Generalization of two-dimensional theories of laminated composite plates. Comm Appl Numer Methods 1987;3:173–80.

[12] Toledano A, Murakami H. A composite plate theory for arbitrary laminate configuration. J Appl Mech 1987;54:181–9.

[13] Lu X, Liu D. An interlaminar shear stress continuity theory for both thin and thick composite laminates. J Appl Mech 1992;59:502–9.

[14] Lee CY, Liu D. An interlaminar stress continuity theory for laminated composite analysis. Comput Struct 1992;42(1):69–78.

[15] DiSciuva M. Development of an anisotropic multilayered shear deformable rectangular plate element. Comput Struct 1985;21:789–96.

[16] DiSciuva M. An improved shear-deformation theory for moderately thick multilayered anisotropic shells and plates. J Appl Mech 1987;54:589–96.

[17] DiSciuva M. A general quadrilateral multilayered plate element with continuous interlaminar stresses. Comput Struct 1993;47:91–105.

[18] Cho M, Parmerter RR. Efficient higher order composite plate theory for general lamination configurations. AIAA J 1993;31:1299–306.

[19] Murakami H. Laminated composite theory with improved in-plane response. J Appl Mech 1986;53:661–6.

[20] Averill RC. Static and dynamic response of moderately thick laminated beams with damage. Composite Eng 1994;4:381–95.

[21] Averill RC, Yip YC. Development of simple, robust finite elements based on refined theories for thick laminated beams. Comput Struct 1996;59:529–46.

[22] Averill RC, Yip YC. An efficient thick beam theory and finite element model with zig-zag sublaminate approximations. AIAA J 1996;34:1627–32.

[23] Yip YC, Averill RC. A 3D laminated plate finite element with zig-zag sublaminate approximations, submitted.

[24] Reissner E. On a mixed variational theorem and on shear deformation plate theory. Int J Numer Methods Eng 1986;23:193–8.

[25] Tessler A, Hughes TJR. An improved treatment of transverse shear in the mindlin-type four-node quadrilateral element. Comput Methods Appl Mech Eng 1983;39:311–35.

[26] Prathap G, Somashekar BR. Field- and edge-consistency synthesis of a 4-noded quadrilateral plate bending element. Int J Numer Methods Eng 1988;26:1693–708.

[27] Burton WS, Noor AK. Three-dimensional solutions for thermomechanical stresses in sandwich panels and shells. J Eng Mech ASCE 1994;120(10):2044–71.

[28] Barlow J. Optimal stress locations in finite element models. Int J Numer Methods Eng 1976;10:243–51.